ELSEVIER

Computers and Chemical Engineering 26 (2002) 1103–1116

Computers & Chemical Engineering

www.elsevier.com/locate/compchemeng

Optimal control and simulation of multidimensional crystallization processes

David L. Ma [a], Danesh K. Tafti [b], Richard D. Braatz [a,*]

[a] *Department of Chemical Engineering, University of Illinois at Urbana-Champaign, 600 South Mathews Avenue, Box C-3, Urbana, IL 61801–3792, USA*

[b] *Mechanical Engineering Department, Virginia Polytechnic Institute and State University, 114 Randolph Hall, Blacksburg, VA 24061, USA*

Accepted 22 February 2002

Abstract

The optimal batch control of a multidimensional crystallization process is investigated. A high resolution algorithm is used to simulate the multidimensional crystal size distribution under the operations defined by two optimal control trajectories. It is shown that a subtle change in the optimal control objective can have a very large effect on the crystal size and shape distribution of the product crystals. The effect of spatial variation is investigated using a compartmental model. The effect of differing numbers of compartments on the size and shape distribution of the product crystals is investigated. It is shown that the crystal size distribution can be very different along the height of the crystallizer and that a solution concentration gradient exists due to imperfect mixing. The nucleation rate can be significantly larger at the bottom of the crystallizer and the growth rate can be much larger at the top. The high resolution method provides high simulation accuracy and fast speed, with the ability to solve large numbers of highly nonlinear coupled multidimensional partial differential equations over a wide range of length scales. A parallel programming implementation results in simulation times that are short enough for using the simulation program to compute optimal control trajectories. © 2002 Elsevier Science Ltd. All rights reserved.

Keywords: Optimal control; Crystallization; Robustness analysis; Batch control; Dynamic programming

---

1. Introduction

Crystallization from solution is an industrially important unit operation due to its ability to provide high purity separations. For efficient downstream operations and product effectiveness, controlling the crystal size and shape distribution can be critically important. This is especially true for the multidimensional crystals produced in the pharmaceutical and photographic industries.

This paper investigates the effectiveness of optimal control for providing the desired product characteristics for a batch crystallization process with multiple growth axes. A high resolution algorithm accurately simulates the multidimensional population balance equation along the optimal control trajectories. While not well known in the crystallization or control communities, high resolution algorithms have been used in the computational physics community for a wide variety of applications (Harten, 1983; LeVeque, 1992, 1997; Osher & Chakravarthy, 1984; Sweby, 1984; Yang, Huang, & Tsuei, 1995). High resolution algorithms can provide second-order accuracy without the spurious oscillations that naive second-order methods usually exhibit, while also reducing numerical diffusion inherited by first-order methods. The wide range of length scales inherent in crystallization processes makes these numerical issues especially critical.

This paper also investigates the effect of spatial variations on the multidimensional crystal size distribution. In batch crystallization, the crystal product characteristics are determined by the seed characteristics, the supersaturation profile, and the mixing conditions. The compartmental modeling approach can be used to take imperfect mixing into account (Braatz & Hasebe, in press, Kramer, Dijkstra, Neumann, Meadhra, & van

---

* Corresponding author. Tel.: +1-217-333-5073; fax: +1-217-333-5052

E-mail address: braatz@uiuc.edu (R.D. Braatz).

PII: S0098-1354(02)00033-9

Rosmalen, 1996). The crystallizer is subdivided into a finite number of smaller sections (called compartments). Perfect mixing is assumed in each compartment. Each compartment has input and output streams that share flows with its neighbors. The quantity of crystals and the crystal characteristics in the input and output streams are governed by the local hydrodynamic conditions. The compartment model enables a much more accurate modeling of the formation of new crystals, which is key to quantifying the quality of the crystal size distribution of the final product. This approach is computationally feasible using today's computer hardware, whereas the full solution of the fluid and particle momentum equations is too computationally intensive, at least for design or control purposes in which multiple simulations are required.

The paper is organized as follows. The model of a KH_2PO_4–H_2O crystallizer is presented first, then the optimal control formulation for two-dimensional crystallization is introduced, followed by a summary of the compartmental modeling approach and the high resolution method, and the results, discussion, and conclusions.

2. Multidimensional crystallization: well-mixed case

While the following description of multidimensional crystallization is rather general, potassium dihydrogen phosphate (KH_2PO_4, KDP) is used to illustrate the key ideas. The shape of KDP crystals is tetragonal prism in combination with tetragonal bipyramid, and the angle between the prism sides and pyramid faces is 45° (Mullin & Amatavivadhana, 1967). The two internal dimensions r_1 and r_2 are the width and length of the KDP crystal, respectively (Fig. 1). Accordingly, the volume of a single crystal is

$$V_c = \frac{1}{3} r_1^3 + (r_2 - r_1) r_1^2. \tag{1}$$

For a well-mixed batch crystallizer in which the crystals have two characteristic length scales, the process is described by the multidimensional population balance equation (Hulburt & Katz, 1964; Randolph & Larson, 1988):

$$\frac{\partial f(r_1, r_2, t)}{\partial t} + \sum_{j=1}^{2} \frac{\partial \{G_j(r_1, r_2, c(t), T(t)) f(r_1, r_2, t)\}}{\partial r_j} = h(f(r_1, r_2, t), c(t), T(t)) \tag{2}$$

where f is crystal size distribution, r_j refers to each characteristic length scale, G_j refers to the growth rate for the jth length scale, c is the solute concentration, and h describes the crystal creation mechanisms. The temperature is described by an energy balance for the crystal slurry (the crystals are small enough that their temperature is equal to the temperature of the surrounding liquid), which is a function of the overall heat transfer coefficient, the heat of crystallization, the crystallization kinetics, and the mass of chemical species transferred between the solution and crystal phases. In practice, this temperature is the setpoint trajectory for a feedback control system that manipulates a valve for a flow to a jacket on the crystallizer. The solution concentration is specified by a material balance on the solution phase, given later.

For KDP, the growth rates are independent of the width and length of the crystals. For the range of temperature considered in this study, the growth rates G_1 and G_2 are functions only of the solute concentration c and the saturated solute concentration c_{sat} (Gunawan, Ma, Fujiwara, & Braatz, in press):

$$G_1(c(t), T(t)) = k_{g_1} \left(\frac{c(t) - c_{sat}(T)}{c_{sat}(T)} \right)^{g_1} = k_{g_1} S^{g_1} \tag{3}$$

$$G_2(c(t), T(t)) = k_{g_2} \left(\frac{c(t) - c_{sat}(T)}{c_{sat}(T)} \right)^{g_2} = k_{g_2} S^{g_2}, \tag{4}$$

where S is the relative supersaturation, and g_1, g_2, k_{g_1}, and k_{g_2} are kinetic parameters. The saturated solute concentration for KDP is given by Togkalidou, Fujiwara, Patel, & Braatz, 2000, 2001

$$c_{sat}(T) = 9.3027 \times 10^{-5} T^2 - 9.7629 \times 10^{-5} T + 0.2087, \tag{5}$$

where T is the temperature in Celsius. Secondary nucleation is the dominant mechanism for producing new crystals in most seeded batch crystallizers. This type of

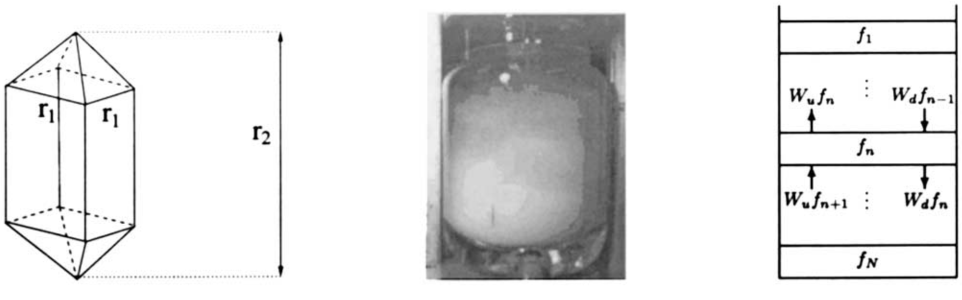

Fig. 1. A KDP crystal, a batch laboratory crystallizer, and its simulation model with N compartments.

Table 1
Kinetic parameters determined from laboratory data (Gunawan et al., in press)

Parameters	Values	Units
g_1	1.48	Dimensionless
k_{g_1}	12.21	μm/s
g_2	1.74	Dimensionless
k_{g_2}	100.75	μm/s
b	2.04	Dimensionless
k_b	7.49×10^{-8}	particles/μm^3 s

nucleation kinetics is usually characterized as being proportional to either the area or volume of crystals in the crystallizer. For the range of temperature considered in this study, the nucleation kinetics for KDP are (Gunawan et al, in press):

$$h(f(r_1,r_2,t),c(t),T(t)) = k_b\left(\frac{c-c_{\mathrm{sat}}}{c}\right)^b \delta(r_1)\delta(r_2)\int_0^\infty\int_0^\infty f(r_1,r_2,t)V_c(r_1,r_2)\mathrm{d}r_1\mathrm{d}r_2 \tag{6}$$

where δ is the Dirac delta function. This assumes that nucleated crystals are small enough to have negligible size. The validity of this assumption has been confirmed by re-simulating the crystallization process with a range of realistic nuclei dimensions and observing that the results are not affected.

A solute mass balance completes the model for a batch crystallizer. With the assumption that nucleated crystals have negligible size, the amount of solute leaving the solution must be accounted by crystal growth. For KDP this equation is

$$\frac{\mathrm{d}c(t)}{\mathrm{d}t} = -\rho_c\int_0^\infty\int_0^\infty f(r_1,r_2,t) \times (2G_1(c(t),T(t))(r_1r_2-r_1^2)+G_2(c(t),T(t))r_1^2) \times \mathrm{d}r_1\mathrm{d}r_2 \tag{7}$$

where ρ_c is the crystal density ($\rho_c = 2.338\times10^{-12}$ g/μm^3 n the simulation). Table 1 summarizes the parameter values in Eq. (3)–Eq. (6), which were determined using parameter estimation and model-based experimental design (Chung, Ma, & Braatz, 2000, 1999a; Ma, Chung, & Braatz, 1999; Matthews & Rawlings, 1998; Miller & Rawlings, 1994).

The following analysis also uses cross-moments which are defined as

$$\mu_{ij}(t) = \int_0^\infty\int_0^\infty f(r_1,r_2,t)r_1^ir_2^j\mathrm{d}r_1\mathrm{d}r_2. \tag{8}$$

The low order moments have physical meaning. For example, μ_{00} is the total number, μ_{10} is the total width, and μ_{01} is the total length of the crystals in the system per gram of solvent. Hence the average width of crystals is μ_{10}/μ_{00}, and the average length is μ_{01}/μ_{00}.

3. Optimal control for a well-mixed crystallizer

In a well-mixed batch KDP crystallizer, the final crystal product is determined by the supersaturation profile, the initial seed mass, and the seed crystal size distribution. In this paper, we only consider the case where supersaturation is created by reducing the temperature $T(t)$, although other methods of achieving supersaturation such as antisolvent addition (Charmolue & Rousseau, 1991) can be formulated in a similar manner. Based on a past study, the effect of the width of the seed crystal size distribution is not as important as the effect of the seed mass (Chung, Ma, & Braatz, 1999b). Also, in practice changing the seed mass is much easier than varying the seed crystal size distribution, which would require an additional unit operation, such as milling (which creates undesirable fines) and/or screening. Here the shape of the initial seed distribution is fixed to

$$f(r_1,r_2,0) = -0.00034786r_1^2+0.1363609r_1-0.00034786r_2^2 + 0.1363609r_2-26.5486 \tag{9}$$

for $180<r_1<220$ and $180<r_2<220$, and zero otherwise. This distribution is multiplied by a scalar to achieve a specified initial seed mass M_{seed}. This is based on crystals that are readily available in the laboratory. Hence the optimal control variables are the seed mass and the temperature profile. The optimal control formulation is

$$\begin{aligned} &\underset{T(t),\ M_{\mathrm{seed}}}{\text{optimize}} \quad \Phi \\ &\text{subject to}\quad g_1(t) = T_{\min}-T(t)\leqslant 0 \\ &g_2(t) = T(t)-T_{\max}\leqslant 0 \\ &g_3(t) = \frac{\mathrm{d}T(t)}{\mathrm{d}t}-R_{\max}\leqslant 0 \\ &g_4(t) = R_{\min}-\frac{\mathrm{d}T(t)}{\mathrm{d}t}\leqslant 0 \\ &g_5 = c(t_{\mathrm{final}})-c_{\max}\leqslant 0 \end{aligned} \tag{10}$$

where Φ is some desired characteristic of the crystals at the end of the batch (details below), which is computed using a cross-moments model (Gunawan et al., in press). The temperature constraints $g_1(t)$–$g_4(t)$ ensure that the temperature profile stays within the operating range of the crystallizer. The constraint g_5 is the minimum yield constraint, as the final solute concentration specifies the amount of crystals produced. This optimal control problem is solved by a successive quadratic program (Zhou, Tits, & Lawrence, 1989) that iteratively calls the cross-moments model.

To the authors' knowledge, the optimal control objectives for multidimensional crystallization have not been investigated in the literature, whereas several objectives have been recommended to favor downstream operations or product quality for one-dimensional crystallizers (Ajinkya & Ray, 1974; Braatz & Hasebe, in press, Eaton & Rawlings, 1990; Jones, 1974; Rawlings, Miller, & Witkowski, 1993). These objectives can be used for multidimensional crystallization with slight modification. Controlling the aspect ratio of two-dimensional crystals can be another useful optimal control objective (Ma & Braatz, 2001).

In this paper, two optimal control objectives are investigated—maximizing the number-weighted average length of the crystal and maximizing the mass-weighted average length of the crystals. While both objectives are based on average length, the different weighting has a significantly different dependence on the size of the crystals. Because the small crystals have a significant effect on the number-weighted average length, it would be expected that maximizing this optimal control objective would keep the number of nucleated crystals as small as possible. The mass-weighted average length is affected very little by small crystals. Both objectives can be calculated directly from the cross-moments:

Objective 1: number-weighted average length,

$$r_2 = \frac{\mu_{01}}{\mu_{00}} \tag{11}$$

Objective 2: mass-weighted average length,

$$r_2 = \frac{\mu_{22} - \frac{2}{3}\mu_{31}}{\mu_{21} - \frac{2}{3}\mu_{30}}. \tag{12}$$

4. Compartmental model

Perfect mixing is rarely true in practice. A 2-l batch crystallizer is shown in Fig. 1. The crystal size distribution f varies substantially along the height of the crystallizer. Due to gravity, most crystals stay at the bottom of the crystallizer while smaller crystals tend to flow with the water and can be seen in the middle and upper regions. Few crystals are located near the top of the slurry.

Compartmental modeling has been used to take spatial variations into account in one-dimensional crystallizers (Braatz & Hasebe, in pressKramer et al., 1996). As suggested from Fig. 1, the crystallizer can be subdivided into smaller compartments. Each compartment is assumed to be well-mixed, that is, the nucleation and growth kinetics are uniform throughout the compartment, and consequently a modification of Eq. (2) can be applied to each compartment. The amount of crystals and the crystal size distribution may be different in each compartment.

Using a larger number of compartments can result in a more accurate model of the system. Each compartment has input and output streams that share flows with its neighbors. The crystal size distribution in those streams is governed by the local conditions. The smallest crystals will flow along streamlines; therefore, the distribution for the smallest crytstals in the output streams of the nth compartment should be equal to the distribution inside the nth compartment. On the other hand, the downward output stream of the nth compartment will have bigger crystals than the upward output stream, when the crystals have a higher density than the fluid. Two weighting functions W_d and W_u are used to characterize these distributions. The crystal size distributions are $W_d f_n$ and $W_u f_n$ in the downward and upward output streams of the nth compartment, where f_n is the crystal size distribution in the nth compartment and

$$W_u = 1.0 - \frac{\beta_1 r_1}{\max(r_1, r_2)} - \frac{\beta_2 r_2}{\max(r_1, r_2)}, \tag{13}$$

$$W_d = 1.0 + \frac{\beta_1 r_1}{\max(r_1, r_2)} + \frac{\beta_2 r_2}{\max(r_1, r_2)}. \tag{14}$$

The constants β_1 and β_2 can be determined from experiments, and r_1 and r_2 are the characteristic length scales for the crystals. For the nth compartment, the population balance equation is

$$\begin{aligned}\frac{\partial f_n}{\partial t} &+ \sum_{j=1}^{2} \frac{\partial\{G_j(c(t),T(t))f_n\}}{\partial r_j} \\ &= h(f_n, c(t), T(t)) \\ &\quad + \frac{F}{V_n}(W_d f_{n-1} + W_u f_{n+1} - W_u f_n - W_d f_n)\end{aligned} \tag{15}$$

where F is the flow rate of input and output streams, V_n is the volume of the compartment n, and each f_n is a function of r_1, r_2, and t. A high resolution algorithm that solves this system of highly nonlinear coupled partial differential equations is discussed next.

5. A high resolution algorithm

The population balance equation Eq. (15) is a multidimensional conservation equation with widely varying length scales (very small to 100s of microns). Solving this equation presents great challenges to naive first-order and second-order finite difference algorithms. In the literature, the first-order approximation methods are often used with special consideration of mesh size in order to reduce numerical diffusion (Sotowa, Naito, Kano, Hasebe, & Hashimoto, 2000). The most popular higher order approximation methods give spurious oscillations, which can result in a population density of crystals with negative values.

High resolution methods have been developed primarily by the computational physics community (Harten, 1983; LeVeque, 1992, 1997; Osher & Chakravarthy, 1984; Sweby, 1984). These methods can well handle large gradients and can give second-order accuracy without producing spurious oscillations or smeared solutions. This motivates the use of such algorithms for the simulation of crystallization. The first step of the algorithm is to solve the homogeneous equation

$$\frac{\partial f}{\partial t}+\sum_{j=1}^{2}\frac{\partial\{G_j[c(t),T(t)]f\}}{\partial r_j}=0 \tag{16}$$

over time step k, then add the crystals on the right hand side of Eq. (15) to the corresponding cells over the same time increment (LeVeque). To handle the multiple crystal dimensions in Eq. (16), a splitting method is used to decompose (Eq. (16)) into a pair of 1D equations, each of which is solved by a high resolution method. Since the algorithm is applied in the same manner to different compartments, the index n will be dropped to simplify notation, and the description will be with respect to a single compartment.

For the 1D wave equation, the grid points are defined as the points $(t_m, r_p)=(mk, ph)$ for positive integers m and p, where h is the mesh size and k is the time step. Fix the ratio of k and h to be constant. Let $f_p{}^m$ be the population density function f defined on the grid point (t_m, r_p).

First we will describe how Eq. (16) can be reduced to two one-dimensional partial differential equations. At the time instant t_{m-1}, this equation is

$$\frac{\partial f}{\partial t}+g_1^{m-1}\frac{\partial f}{\partial r_1}+g_2^{m-1}\frac{\partial f}{\partial r_2}=0 \tag{17}$$

with initial crystal size distribution

$$f=f^{m-1}(r_1,r_2). \tag{18}$$

The analytical solution to this PDE at t_m is

$$f=f^{m-1}(r_1-g_1^{m-1}(t_m-t_{m-1}),r_2-g_2^{m-1}(t_m-t_{m-1})) \tag{19}$$

Now recognize that the same PDE can also be solved in two steps. First, solve the 1D PDE

$$\frac{\partial \hat{f}}{\partial t}+g_1^{m-1}\frac{\partial \hat{f}}{\partial r_1}=0 \tag{20}$$

$$\hat{f}=f^{m-1}(r_1,r_2) \quad \text{at} \quad t=t_{m-1}. \tag{21}$$

The solution to this PDE is $\hat{f}^m(r_1,r_2)=f^{m-1}(r_1-g_1^{m-1}(t_m-t_{m-1}),r_2)$. Now use the obtained $\hat{f}$ as the initial condition to solve the second PDE,

$$\frac{\partial \tilde{f}}{\partial t}+g_2^{m-1}\frac{\partial \tilde{f}}{\partial r_2}=0 \tag{22}$$

$$\tilde{f}=\hat{f}^m(r_1,r_2) \quad \text{at} \quad t=t_{m-1}. \tag{23}$$

The solution to the second PDE at t_m is Eq. (19) since

$$\begin{aligned}\tilde{f}(r_1,r_2)&=\hat{f}^m(r_1,r_2-g_2^{m-1}(t_m-t_{m-1}))\\&=f^{m-1}(r_1-g_1^{m-1}(t_m-t_{m-1}),r_2-g_2^{m-1}(t_m-t_{m-1})).\end{aligned} \tag{24}$$

This derivation shows that the 2D PDE Eq. (16) can be solved by first splitting it to a pair of 1D PDEs along r_1 and r_2, and then solving the two PDEs consecutively at each time step. Then the two solutions can be combined to form the solution to the original PDE.

With Eq. (16) split into a pair of 1D equations, at each time instant a PDE in the form of

$$\frac{\partial f}{\partial t}+g\frac{\partial f}{\partial r}=0 \tag{25}$$

must be solved with the initial condition $f(r)=\bar{f}(r)$. High resolution methods are specially suitable for solving this equation (LeVeque, 1992).

This paper will use a high resolution method that is essentially a hybrid of the upwind method and the Lax–Wendroff method. The upwind method is a first-order finite difference method. It replaces $\partial f/\partial t$ by a forward-in-time approximation and $\partial f/\partial r$ by a backward finite difference. The difference equation obtained for $f_p{}^{m+1}$ is

$$f_p^{m+1}=f_p^m-\frac{k}{h}g(f_p^m-f_{p-1}^m). \tag{26}$$

The main drawback of this method is that it exhibits severe numerical diffusion. The Lax–Wendroff method on the other hand gives second-order accuracy and reduces the numerical diffusion:

$$\begin{aligned}f_p^{m+1}=&f_p^m-\frac{kg}{2h}(f_{p+1}^m-f_{p-1}^m)\\&+\frac{k^2g^2}{2h^2}(f_{p+1}^m-2f_p^m+f_{p-1}^m).\end{aligned} \tag{27}$$

The drawback of this method is that it introduces spurious oscillations. The population density can have negative values when the local gradients are large, which occurs in crystallization processes. Rewriting the Lax–Wendroff method in the following form provides insight into the cause of oscillation:

$$\begin{aligned}f_p^{m+1}=&f_p^m-\frac{kg}{h}(f_p^m-f_{p-1}^m)\\&-\frac{kg}{2h}\left(1-\frac{kg}{h}\right)[(f_{p+1}^m-f_p^m)-(f_p^m-f_{p-1}^m)].\end{aligned} \tag{28}$$

Eq. (28) shows that the Lax–Wendroff method consists of the first-order upwind method, supplemented with an anti-diffusion term

$$\frac{kg}{2h}\left(1-\frac{kg}{h}\right)((f^m_{p+1}-f^m_p)-(f^m_p-f^m_{p-1})). \tag{29}$$

This anti-diffusion term prevents the diffusion, but the magnitude of this term might be too large, causing spurious oscillations. To remedy this, the high resolution method restricts the magnitude of this anti-diffusion term:

$$f^{m+1}_p = f^m_p - \frac{kg}{h}(f^m_p - f^m_{p-1}) - \frac{kg}{2h}\left(1-\frac{kg}{h}\right)((f^m_{p+1}-f^m_p)\phi_p-(f^m_p-f^m_{p-1})\phi_{p-1}). \tag{30}$$

The term ϕ_p is called a limiter, whose value depends on the local gradients. Define θ_p as the ratio of the local gradients

$$\theta_p = \frac{f^m_p - f^m_{p-1}}{f^m_{p+1} - f^m_p} \tag{31}$$

and let ϕ_p be a function of the local gradients so that $\phi_p = \phi(\theta_p)$. The limiter function ϕ is selected so that the difference approximation is consistent with Eq. (25) and does not produce any spurious oscillation. It is also desired for the limiter to give a difference approximation that is second-order accurate. It can be shown that the limiter function ϕ satisfies the above requirements if $\phi(1) = 1$ with ϕ Lipschitz continuous at $\theta = 1$, and ϕ satisfies the constraints (LeVeque, 1992; Sweby, 1984):

$$0 \leqslant \frac{\phi(\theta_p)}{\theta_p} \leqslant 2 \tag{32}$$

and

$$0 \leqslant \phi(\theta_p) \leqslant 2. \tag{33}$$

Many choices for the limiter function ϕ are available, and detailed comparison have been made (Sweby, 1984; Zalesak, 1987). This paper found good results using the limited function (van Leer, 1974)

$$\phi(\theta_p) = \frac{|\theta_p| + \theta_p}{1 + |\theta_p|}. \tag{34}$$

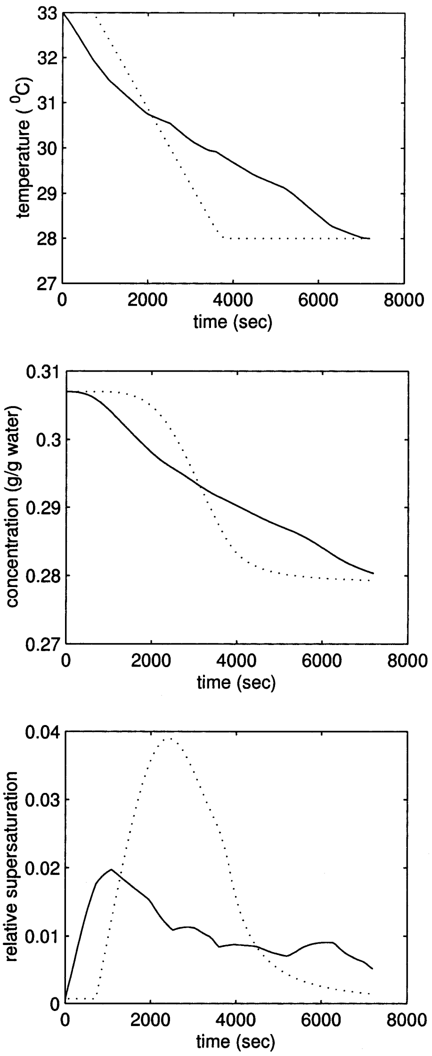

Fig. 2. The temperature, solution concentration, and relative supersaturation profiles that maximize the number-weighted average length (objective 1, —) and the mass-weighted average length (objective 2, ···).

Table 2
Final objective values

	Number-averaged r_2 (μm)	Mass-averaged r_2 (μm)
Objective 1	334	484
Objective 2	297	855

6. Results and discussion

An optimal control study is followed by a consideration of the effects of spatial variation on the multidimensional crystal size distribution.

6.1. Optimal control study

Fig. 2 shows the optimal temperature, the solution concentration, and the relative supersaturation profiles for the two objectives. Table 2 gives the final objective values. For objective 1, the cooling rate is more nearly uniform during the crystallization run. The solution concentration decreases nearly linearly during the batch run, and the relative supersaturation is kept relatively small (< 0.02). For objective 2, the temperature is kept constant initially, then it is dropped as fast as possible, then it is kept constant at its final value throughout the

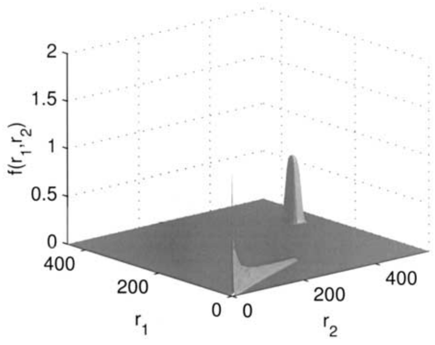

Fig. 3. Final crystal size distribution with optimal control objective 1.

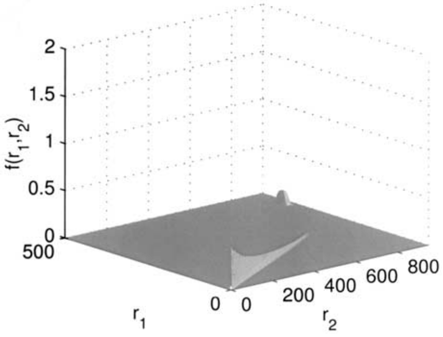

Fig. 4. Final crystal size distribution with optimal control objective 2.

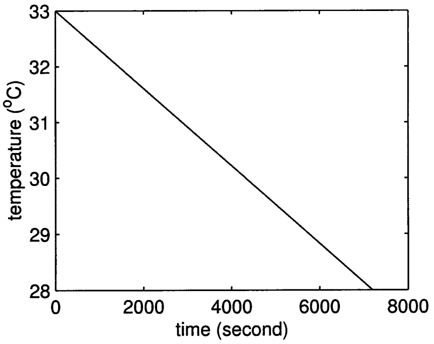

Fig. 5. Temperature profile of the batch crystallizer.

Table 3
Parameters used in simulation

Variable	Description	Value	Units
k	Time step	1	s
h	Mesh size	1	μm
F	Flow rate	10	cc/s
V	Volume	2	l
t	Batch time	2	h
β_1	Coefficient	0.1	None
β_2	Coefficient	0.1	None
M_{seed}	Seed mass	0.02	g/g water

rest of the batch run. This temperature trajectory generates larger relative supersaturation during the second quarter of the batch run. The optimal seed mass for objective 1 is 0.08 g/g solvent, and for objective 2 is 0.016 g/g solvent.

These results are related to an observation made in an earlier study, that the optimal control objective must be selected very carefully for the resulting operations to give the desired product (Chung et al., 1999b). In particular, a past study showed that using the coefficient of variation, which has been used in a number of past optimal control studies, can easily lead to undesirable batch operations. Similarly, a number of weighted average characteristic lengths have been studied in past studies. Above it is demonstrated that the weighting used to define the average length can have a significant effect on the optimal control trajectory. Because of this, it is important when evaluating optimal control trajectories to simulate the entire crystal size distribution, rather than just a simple moment model as is commonly done in the literature. Simulation of the crystal size distribution enables an understanding of the optimal control results (such simulations were used to reach the conclusions in the last paragraph), which can be used to develop an improved optimal control formulation.

The well-mixed batch crystallizer operating under the two optimal control trajectories was simulated using the high resolution method. The final crystal size distributions for the two objectives are plotted in Fig. 3 and Fig. 4. Comparing these two figures, the seed crystals are much fewer and larger for objective 2; however, objective 2 also gives a wider variation in size for the crystals growth from nuclei. Objectives 1 and 2 have different tradeoffs between the mechanisms of nucleation and growth, which could have a significant effect on downstream processing (Togkalidou, Braatz, Johnson, Davidson, & Andrews, 2001).

6.2. Effect of spatial variations

When considering the imperfect mixing case, first consider the case where the KH_2PO_4–H_2O crystallizer is subdivided into eight compartments. The eighth compartment is at the bottom of the crystallizer; the sixth, fourth, and second compartments are one, two, and three quarters above the bottom, respectively. The temperature is uniform throughout the crystallizer. Fig. 5 shows the temperature profile for each compartment. Parameters used in the simulation are summarized in Table 3.

Before the crystallization starts, seed crystals are added into the solution so that secondary nucleation is the dominant nucleation mechanism. The seeds are loaded into the bottom compartment. The average length and width of the seeds are 200 μm. The seed size distribution is given in Fig. 6. After 2 h of crystallization, the crystal size distribution is shown in Fig. 7. The two distributions in each compartment are the crystals grown from seeds and from nuclei. The average length of the crystals grown from seeds is around 800 μm and the average width is around 450 μm, indicating that the crystals are elongating. The size of new nuclei is small (the sharp peak at $r_1 = r_2 = 0$), and as time evolves, the nucleated crystals grow larger. The largest crystals tend to stay at the bottom of the crystallizer. Note that there are no spurious oscillations or significant numerical diffusion observed in Fig. 7.

The final crystal size distribution is a strong function of the number of compartments. Figs. 8–11 show the final crystal size distribution when the number of compartments is changed while keeping the flow rate F and initial seed mass constant. Figs. 12–16 show the corresponding solution concentration and relative supersaturation profiles. Those figures indicate how the concentration gradient develops as more compartments are used. As shown in Fig. 16, the relative supersaturation near the top is nearly five times higher than the one at the bottom. This implies that crystals grow faster in the top compartments. As crystals become larger, they leave the top compartments due to gravity and enter the bottom compartments which are associated with a slower growth rate. At the same time, fresh small crystals enter the top compartments from the bottom. Due to the different growth rates and the circulation inside the crystallizer, the final crystal size distribution is very different from the one when the crystallizer is nearly well-mixed (Fig. 8). When there is a large number of compartments, the distributions of crystals grown from seeds and from nuclei are much broader. An unattentive researcher not realizing that the spatial variations in the crystallizer were significant, could mistakenly conclude that growth dispersion (Randolph & Larson, 1988) was significant in cases when it is not. This implies that researchers studying growth dispersion must be absolutely certain their crystallizer is well-mixed before attempting to quantify the magnitude or type of growth dispersion.

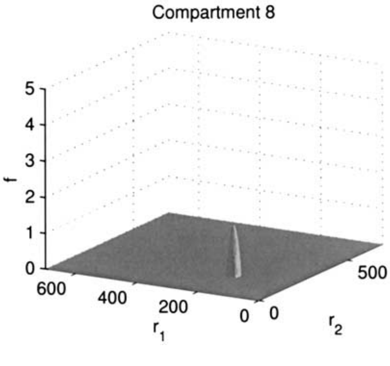
Compartment 8

Fig. 6. Initial seed crystal size distribution when 8 compartments are used.

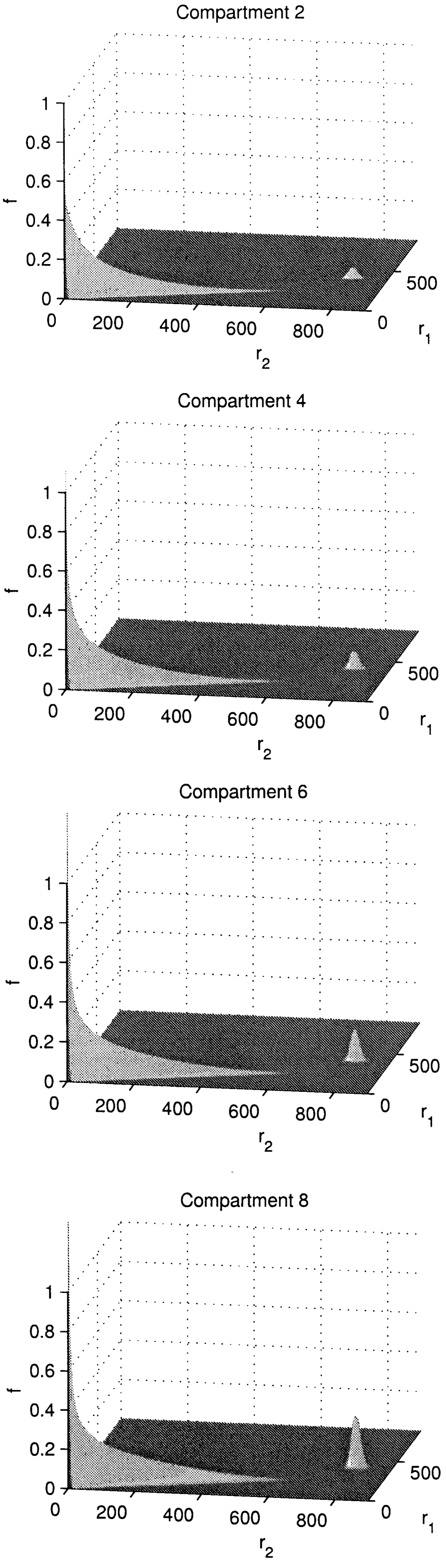
Compartment 2

Compartment 4

Compartment 6

Compartment 8

Fig. 7. Final crystal size distribution when 8 compartments are used.

The nucleation rate is much higher at the bottom of the crystallizer than the top (Fig. 17). For 64 compartments, the nucleation rate at the top is negligible for the first 4000 s, while there is significant nucleation at the bottom of the crystallizer for the entire batch crystallization run. There can be several orders of magnitude variation in nucleation rate across the crystallizer.

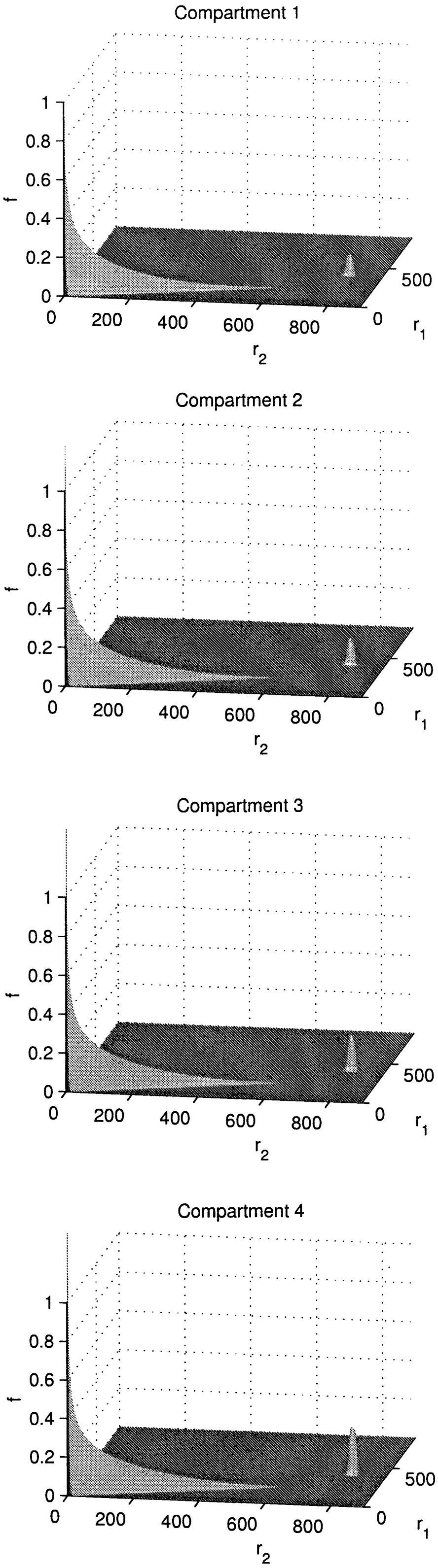
Compartment 1

Compartment 2

Compartment 3

Compartment 4

Fig. 8. Final crystal size distribution when 4 compartments are used.

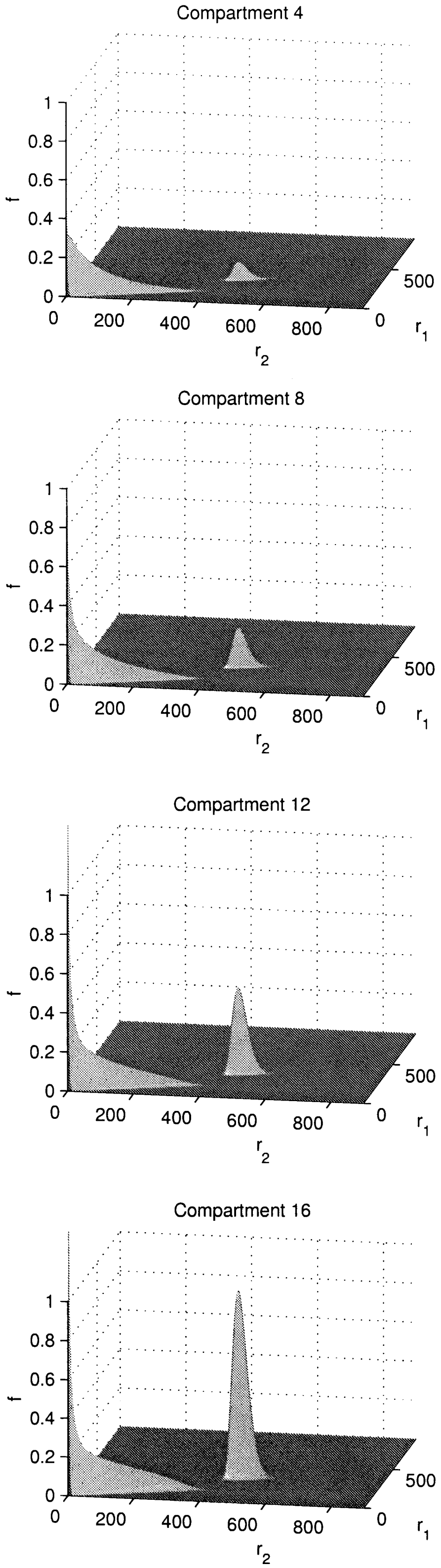
Compartment 4

Compartment 8

Compartment 12

Compartment 16

Fig. 9. Final crystal size distribution when 16 compartments are used.

Increasing the number of compartments makes the simulation time significantly longer if only a single processor handles all computations. Parallel computa-

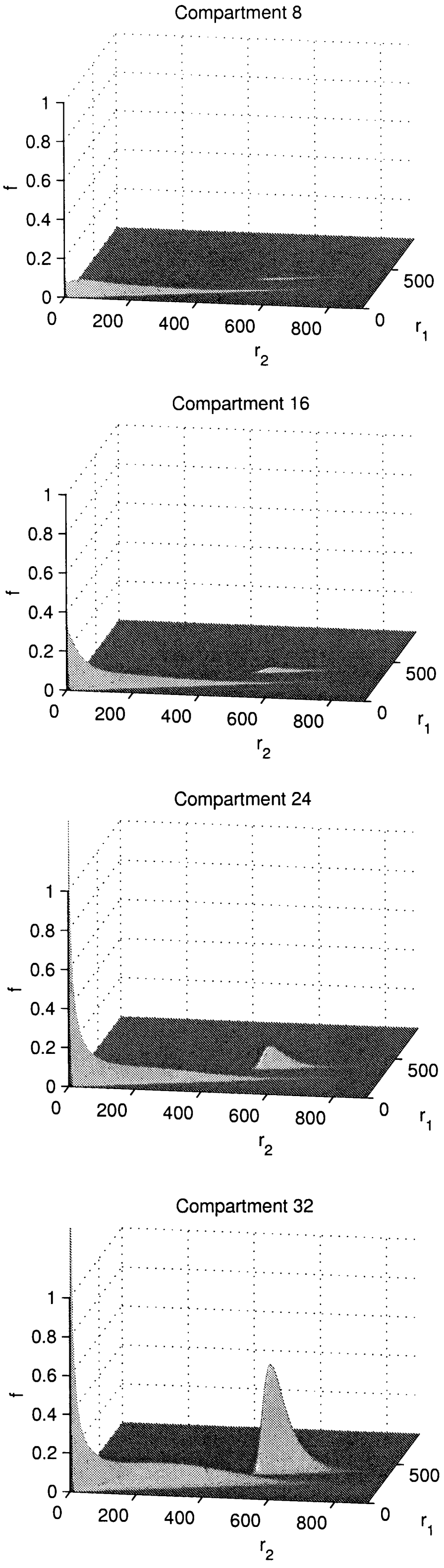

Fig. 10. Final crystal size distribution when 32 compartments are used.

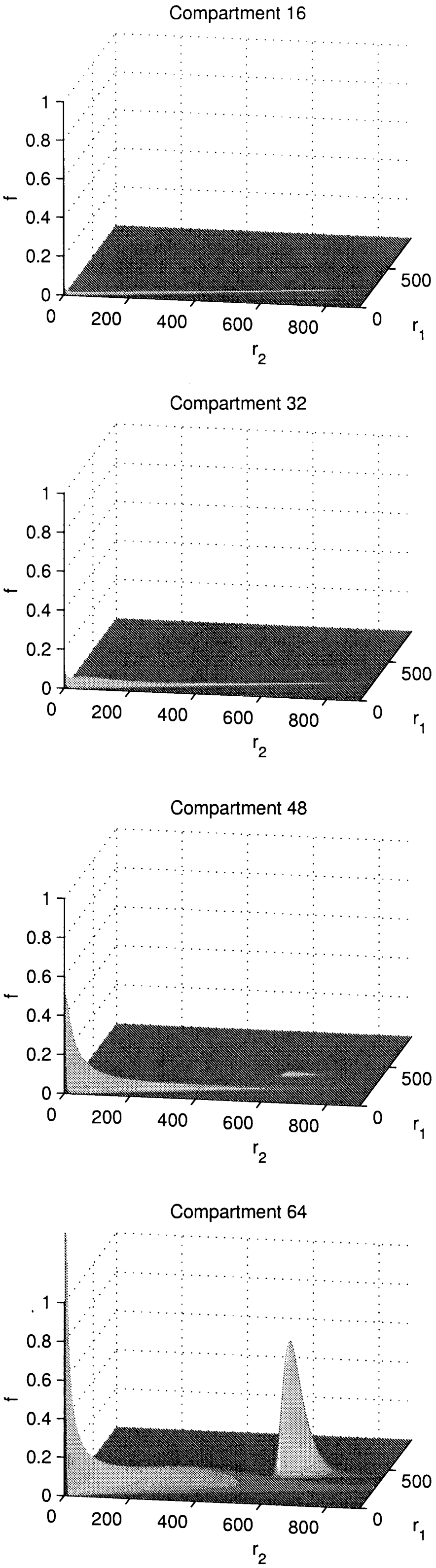

Fig. 11. Final crystal size distribution when 64 compartments are used.

tion was used to speed up the simulation. Each compartment was assigned to a different processor. The task for each processor was to compute the solute concentration and crystal size distribution in the compartment that it was assigned, and then pass this information to its neighboring upper and lower compartments. The simulation time increases as the number of compartments are increased (Table 4) because it

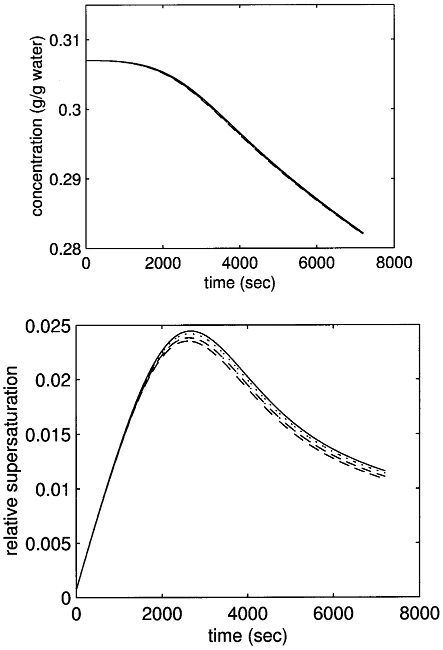

Fig. 12. Concentration and relative supersaturation profiles when 4 compartments are used. The compartments are numbered starting from the top of the crystallizer. The compartment numbers are: 4 (---), 3 (- · -), 2 (···), 1 (—).

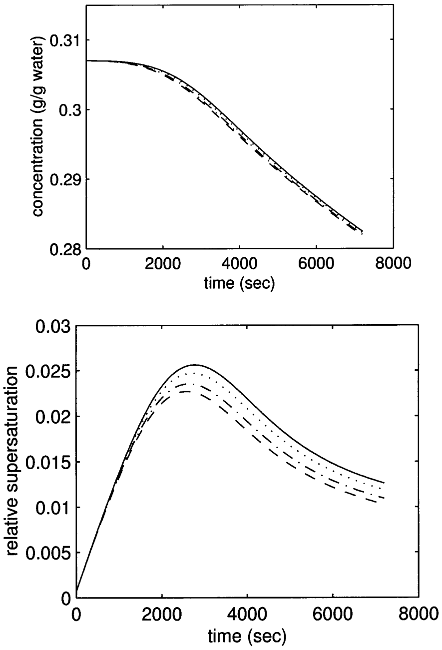

Fig. 13. Concentration and relative supersaturation profiles when 8 compartments are used. The compartments are numbered starting from the top of the crystallizer. The compartment numbers are: 8 (---), 6 (- · -), 4 (···), 2 (—).

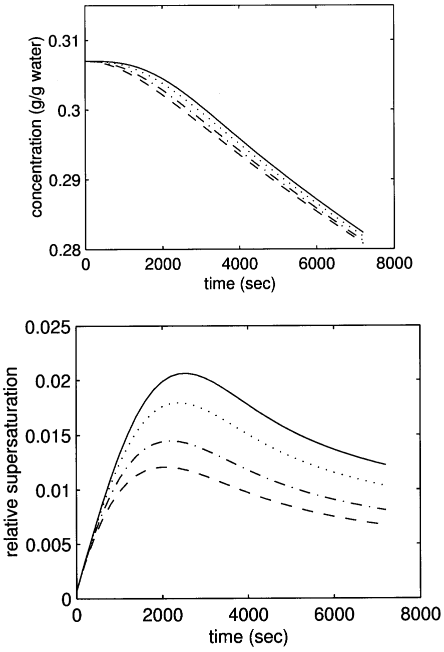

Fig. 14. Concentration and relative supersaturation profiles when 16 compartments are used. The compartments are numbered starting from the top of the crystallizer. The compartment numbers are: 16 (---), 12 (- · -), 8 (···), 4 (—).

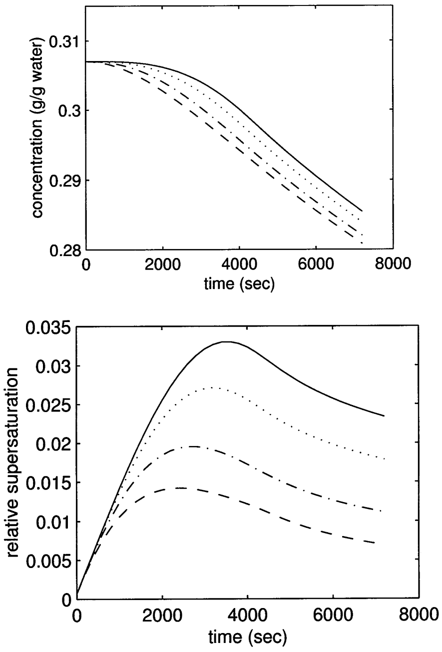

Fig. 15. Concentration and relative supersaturation profiles when 32 compartments are used. The compartments are numbered starting from the top of the crystallizer. The compartment numbers are: 32 (---), 24 (- · -), 16 (···), 8 (—).

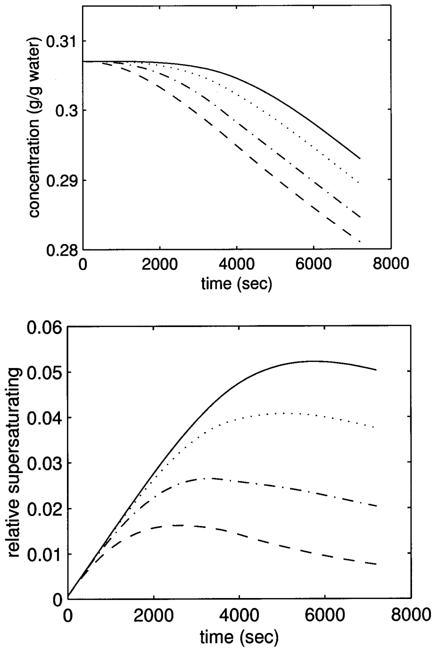

Fig. 16. Concentration and relative supersaturation profiles when 64 compartments are used. The compartments are numbered starting from the top of the crystallizer. The compartment numbers are: 64 (---), 48 (- · -), 32 (···), 16 (—).

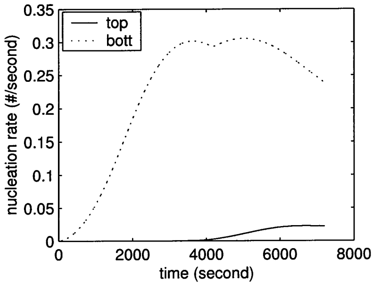

Fig. 17. Nucleation rate at the top and bottom of a batch crystallizer with spatial variation modeled with 64 compartments.

Table 4
Simulation time for different number of compartments

Number of compartments	4	8	16	32	64
Kayak (min)	59	65	75	90	102
Origin (min)	290	326	420	445	470

takes time to pass the information to the neighbors, and because the size of the simulation domain for r_1 and r_2 grows as the number of compartments is increased. The simulations were done on a linux cluster and an Origin 2000. The linux cluster was constructed from HP Kayak Visualize Workstations, each with dual PIII Xeon 550 MHz processors, 512k cache per CPU, and 1GB of memory. Each R10000 processor of the SGI Origin 2000 has 32GB of memory and a clock speed of 195 MHz. The simulation results show that the time increases 15–20% when the number of compartments doubles.

To determine the efficiency in the use of the parallel computer's resources, the individual effects of the domain size and the cost of information transfer on the computation time were determined. The final domain sizes are listed in Table 5. Table 5 reveals that the number of elements increases 51% when the number of compartments triples (from 4 to 64), while the computation time shown in Table 4 increases 62–73%, depending on which parallel computer is used. Hence almost all of the increase in computation time as the number of compartments increases is due to the increase in domain size. The parallel efficiencies up to 64 processors are 85 and 93% on the linux cluster and the Origin 2000, respectively.

Hence there is good scaleup and fast results for both parallel computers. This is especially interesting for the linux cluster, as it is relatively inexpensive ($\approx$ \$1000/node). For 64 compartments, the simulation model consists of 64 highly nonlinear coupled multidimensional partial differential equations describing the crystal size distribution that are solved simultaneously with 64 coupled integrodifferential equations describing the solution phase. The computed crystal size distributions exhibits a wide range of spatial length scales, from 1 μm to approximately 1000 μm, with the nucleated crystals being represented by Dirac delta functions. The computation time of 102 min for 64 compartments is quite reasonable for using the simulation to compute optimal control trajectories. A lower order model is preferred for specifying control objectives (as done here), for on-line optimization in model predictive controllers, and for providing initial convergence toward the optimal control trajectory before switching to the more complicated simulation model.

Table 5
Domain sizes for varying numbers of compartments

Number of compartments	4	8	16	32	64
r_1 (μm)	849	883	952	1048	1102
r_2 (μm)	437	446	466	495	508
Number of nodes	372 300	395 148	445 051	520 304	561 427

7. Conclusions

The optimal control of the batch formation of multidimensional crystals was investigated. It was shown that a subtle change in the optimal control objective could have a very large effect on the crystal size and shape distribution of the product crystals. The effect of spatial variation was investigated using a compartmental model. The simulation results show that crystal size distribution can be very different along the height of the crystallizer and a solution concentration gradient exists due to imperfect mixing. The results also show that the nucleation rate is significantly larger at the bottom of the crystallizer and that the growth rate is much larger at the top. A high resolution method provided very satisfactory simulation accuracy and speed. No spurious oscillations or significant numerical diffusion was observed. Parallel programming techniques made it possible to have short simulation times while still using a large number of compartments to represent smooth spatial variations across the crystallizer.

Acknowledgements

Support from the Computational Science and Engineering Program at the University of Illinois is gratefully acknowledged.

References

Ajinkya, M. B., & Ray, W. H. (1974). On the optimal operation of crystallization processes. *Chemical Engineering Communication*, *1*, 181–186.

Braatz, R. D., & Hasebe, S. Particle size and shape control in crystallization processes. In: J. B. Rawlings & B. A. Ogunnaike, (Eds.), *Chemical process Control VI*. New York: AIChE Press, in press.

Charmolue, H., & Rousseau, R. W. (1991). L-serine obtained by methanol addition in batch crystallization. *American Institute of Chemical Engineering Journal*, *37*, 1121–1128.

Chung, S. H., Ma, D. L., & Braatz, R. D. (1999a). *FORTRAN software for simulation, parameter estimation, experimental design, and optimal control of batch crystallization*. Urbana: University of Illinois http://brahms.scs.uiuc.edu/lssrl/software/crystal, computer software.

Chung, S. H., Ma, D. L., & Braatz, R. D. (1999b). Optimal seeding in batch crystallization. *Canadian Journal of Chemical Engineering*, *77*, 590–596.

Chung, S. H., Ma, D. L., & Braatz, R. (2000). Optimal model-based experimental design in batch crystallization. *Chemometrics and Intelligent Laboratory Systems*, *50*, 83–90.

Eaton, J. W., & Rawlings, J. B. (1990). Feedback control of chemical processes using on-line optimization techniques. *Computers and Chemical Engineering*, *14*, 469–479.

Gunawan, R., Ma, D. L., Fujiwara, M., & Braatz, R. D. (2002). Identification of kinetic parameters in a multidimensional crystallization process. *International Journal of Modern Physics B*, *16*, 367–374.

Harten, A. (1983). High resolution schemes for hyperbolic conservation laws. *Journal of Computational Physics*, *49*, 357–393.

Hulburt, H. M., & Katz, S. (1964). Some problems in particle technology. *Chemical Engineering Science*, *19*, 555–574.

Jones, A. G. (1974). Optimal operation of a batch cooling crystallizer. *Chemical Engineering Science*, *29*, 1075–1087.

Kramer, H. J. M., Dijkstra, J. W., Neumann, A. M., Meadhra, R. O., & van Rosmalen, G. M. (1996). Modelling of industrial crystallizers, a compartmental approach using a dynamic flowsheeting tool. *Journal of Crystal Growth*, *166*, 1084–1088.

LeVeque, R. J. (1992). *Numerical methods for conservation laws*. Basel, Germany: Birkhäuser Verlag.

LeVeque, R. J. (1997). Wave propagation algorithms for multidimensional hyperbolic systems. *Journal of Computational Physics*, *131*, 327–353.

Ma, D. L., & Braatz, R. D. (2001). Worst-case analysis of finite-time control policies. *IEEE Transactions on Control Systems Technology*, *9*, 766–774.

Ma, D. L., Chung, S. H., & Braatz, R. D. (1999). Worst-case performance analysis of optimal batch control trajectories. *American Institute of Chemical Engineering Journal*, *45*, 1469–1476.

Matthews, H. B., & Rawlings, J. B. (1998). Batch crystallization of a photochemical modeling, control and filtration. *American Institute of Chemical Engineering Journal*, *44*, 1119–1127.

Miller, S. M., & Rawlings, J. B. (1994). Model identification and control strategies for batch cooling crystallizers. *American Institute of Chemical Engineering Journal*, *40*, 1312–1327.

Mullin, J. W., & Amatavivadhana, A. (1967). Growth kinetics of ammonium- and potassium-dihydrogen phosphate crystals. *Journal of Applied Chemistry*, *17*, 151–156.

Osher, S., & Chakravarthy, S. (1984). High resolution schemes and the entropy condition. *SIAM Journal on Numerical Analysis*, *131*, 955–984.

Randolph, A., & Larson, M. A. (1988). *Theory of particulate processes* (2nd ed.). San Diego: Academic Press.

Rawlings, J. B., Miller, S. M., & Witkowski, W. R. (1993). Model identification and control of solution crystallization processes: a review. *Industrial Engineering and Chemical Research*, *32*, 1275–1296.

Sotowa, K., Naito, K., Kano, M., Hasebe, S., & Hashimoto, I. (2000). Application of the method of characteristics to crystallizer simulation and comparison with finite difference for controller performance evaluation. *Journal of Process Control*, *10*, 203–208.

Sweby, P. K. (1984). High resolution schemes using flux limiters for hyperbolic conservation laws. *SIAM Journal on Numerical Analysis*, *21*, 995–1011.

Togkalidou, T., Braatz, R. D., Johnson, B., Davidson, O., & Andrews, A. (2001). Experimental design and inferential modeling in pharmaceutical crystallization. *American Institute of Chemical Engineering Journal*, *47*, 160–168.

Togkalidou, T., Fujiwara, M., Patel, S., & Braatz, R. D., (2000). A robust chemometrics approach to inferential estimation of supersaturation. *Proceedings of the American control conference* (pp. 1732–1736). Piscataway, New Jersey: IEEE Press.

Togkalidou, T., Fujiwara, M., Patel, S., & Braatz, R. D. (2001). Solute concentration prediction using chemometrics and spectroscopy. *Journal of Crystal Growth*, *231*, 534–543.

van Leer, B. (1974). Towards the ultimate conservative difference scheme II. Monotonicity and conservation combined in a second order scheme. *Journal of Computational Physics*, *14*, 361–370.

Yang, J. Y., Huang, J. C., & Tsuei, L. (1995). Numerical solutions of the nonlinear model boltzmann equations. *Proceedings of the Royal Society of London Series A—Mathematical and Physical Science*, *448*, 55–80.

Zalesak, S. T. (1987). A preliminary comparison of modern shockcapturing schemes: linear advection. In R. Vichnevetsky, & R. S. Stepleman, *Advances in computer methods for partial differential equations*, vol. VI (pp. 15–22). New Brunswick, NJ: IMACS.

Zhou, J. L., Tits, A. L., & Lawrence, C. T. (1989). *FFSQP*. College Park: University of Maryland http://www.isr.umd.edu/isr/research/patents.html, computer software.